Journal of Sound and Vibration (1999) **227**(5), 899–913
Article No. jsvi.1999.2981, available online at http://www.idealibrary.com on IDEAL®

A LINEAR WHEEL–TRACK MODEL TO PREDICT INSTABILITY AND SHORT PITCH CORRUGATION

S. MÜLLER
Technical University of Berlin, *Aerospace Institute*, *Marchstr*. 12, 10587 *Berlin*, *Germany**

(*Accepted* 22 *September* 1998)

The aim of this paper is to assist in understanding the formation of short pitch corrugation on railway rails. Based on previous work, a linear mathematical model for the description of the transient wheel–rail dynamics has been set up. To ensure linearity it is proved that the wheel–track model remains stable. For the long-term corrugation process a feedback between transient wheel–rail dynamics and a wear mechanism is assumed. A geometrical filter function is introduced which could explain why corrugation wavelengths observed in practice vary little with train speed. Calculations of the wear process on the rail show how vehicle speed and wheel and rail dynamics modify the corrugation response and how corrugation growth can be reduced.

1. INTRODUCTION

Corrugation of rails has been observed for more than a hundred years and causes unwelcome effects such as noise and damage to the track. A large number of publications has been concerned with the problem and most corrugation types can be explained to date. The mechanism which leads to so-called short pitch corrugation, however, is not yet understood. Nowadays, it is common to blame structural dynamics effects at fixed frequencies for the formation of short pitch corrugation [1, 2]. On the basis of this explanation, the corrugation wavelength should vary in direct proportion to the vehicle speed. This is not observed in practice, however, where the wavelengths vary only slightly with running speed [3]. The aim of the paper presented is to clarify this contradiction.

Based on previous work [2, 4], a linear mathematical model for the description of the transient wheel–rail dynamics has been set up. The model takes into account the discrete support of the rail, elasticity of the wheelset, all six degrees of freedom (DOF) of wheel and rail, transient creepage, shift of the contact point and filter effects at short wavelengths. A feedback between transient

*Postal address from the 4th of May: Asea Brown Boveri AG, Speyerer Straße 4, D-69115 Heidelberg, Germany.

0022–460X/99/450899 + 15 $30.00/0

wheel–rail dynamics and a damage mechanism is assumed for the long-term corrugation process: a wheelset rolls over the initial profile irregularity on the rail. After this wheel passage the rail surface is damaged, which modifies the initial profile irregularity. The next wheelset then rolls over the modified profile which damages the rail surface again.

The first part of this paper shows how the corrugation development can be described by a linear wheel–rail model with three subsystems: contact geometry and kinematics; contact mechanics; wheel and track dynamics.

The relationships between the three subsystems are given and it is investigated whether the wheel–rail model remains stable. After that, the long-term corrugation process is described. A wear model is introduced which allows for the calculation of wear patterns on the rail head and it is investigated how fluctuating wear is affected by geometrical effects. This leads to a geometrical filter function which promotes corrugation within a fixed wavelength band. In the last part, calculations of wear patterns after a high number of wheel passages show how the rail dynamics modify the corrugation response and that corrugation is suppressed when constant creepages are reduced.

2. LINEARIZATION OF WHEEL–TRACK DYNAMICS

Generally, the high frequency interaction between wheel and rail and the long-term corrugation process on the running surface of the rail are non-linear processes. The non-linearity of the wheel–rail interaction is due to the processes within the contact patch. While the dynamic motion of wheel and rail can be assumed to be linear the relations of the rolling contact are generally non-linear. To consider this behaviour properly a non-linear calculation is necessary. However, to avoid difficulties due to variations of parameters, etc., a different approach is used here, which is described in the following.

The description of the interaction between wheel and rail is divided into a reference state and a linearized part which fluctuates about it. The solution of each quantity x is then the superposition of a part x_0 and a fluctuating part $\widetilde{\Delta x}$

$$x = x_0 + \widetilde{\Delta x}.$$

The reference state is regarded as quasi-static with respect to the linearized part. Even low frequency vibrations due to long-wavelength track irregularities or the hunting motion can be treated as quasi-static. Then, however, it must be considered that the reference state is different for every moment of the low frequency motion. The development of a non-linear wheel–rail model for the description of the reference state is not part of this paper. The reference state is calculated numerically with an existing program [5].

The linearized part is excited by the profile irregularity on the rail. The profile irregularity is Fourier analyzed and hence the wheel–rail model can be described in the Fourier domain. The linearized part is $\widetilde{\Delta x} = \Delta x\, \mathrm{e}^{\mathrm{i}(2\pi/L)vt}$, where L is the wavelength of one Fourier part of the disturbance and v is the speed of the wheel rolling over the rail.

Linearity seems to be a reasonable assumption at least for the beginning of the wear process. For increasing profile amplitudes a non-linear model is necessary. Then, however, variations of parameters and general statements are more difficult. Nevertheless, it is not clear up to now if even the beginning is a linear process. In reference [6], for example, it was found that ripples developed due to frequency modulations, which is a non-linear process. In reference [7] the results of a linear corrugation model have been compared with measurements and there was no good agreement. Thus, all results presented here should be verified by measurements. Even if an exact prediction seems to be unlikely, at least tendencies should be described correctly. The verification of the presented wheel–rail model is part of the ongoing project *Silent Track*, funded by the European Railway Research Institute (ERRI) [8].

3. TRANSIENT WHEEL–RAIL DYNAMICS AND FEEDBACK LOOP

A harmonic profile irregularity on the running surface of the rail causes harmonic changes in forces and displacements between wheel and rail. The linear interaction between these fluctuating quantities can be described by a feedback loop. All relationships are given in the following and are summarized in Figure 4 at the end of this section. They are related to the left wheel–rail combination. Irregularities on the wheel are fully neglected.

3.1. CONTACT GEOMETRY

The profile irregularity and relative displacements between wheel and rail can change geometry parameters. The amplitudes of the fluctuating geometry parameters are (cf. Figure 1) Δr, the amplitude of the longitudinal wheel radius, ΔR^r, the amplitude of the lateral rail radius, $\Delta(1/R)$, the amplitude of the longitudinal rail curvature, $\Delta\alpha$, the amplitude of the lateral contact location, Δd, the amplitude of the penetration between wheel and rail, and $\Delta\xi^c$, the amplitude of the longitudinal contact location.

The harmonic profile irregularity on the running surface of the rail is described by

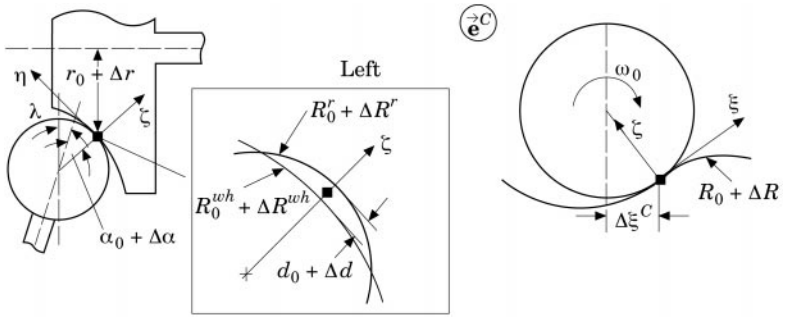

Figure 1. Geometry parameters.

$$\Delta z(x, \eta) = (\Delta z_w + \Delta z_\varphi \eta/b + \Delta z_\kappa(\tfrac{3}{2}(\eta/b)^2 - \tfrac{1}{2}))\, \mathrm{e}^{\mathrm{i}(2\pi/L)x}, \tag{1}$$

where η is the co-ordinate of the contact system $\vec{\mathbf{e}}^C$ in the lateral direction (cf. Figure 1) and $2b$ is the length of the contact patch normal to the rolling direction.

When a wheel is rolling over the disturbance with speed v the wheel–track system is excited by

$$\Delta z(t, \eta) = (\Delta z_w + \Delta z_\varphi \eta/b + \Delta z_\kappa(\tfrac{3}{2}(\eta/b)^2 - \tfrac{1}{2}))\, \mathrm{e}^{\Omega t},$$

with $\Omega = 2\pi v/L$.

The relative displacements are defined as

$$\begin{Bmatrix} \Delta u_x \\ \Delta u_y \\ \Delta u_z \\ \Delta \varphi_x \\ \Delta \varphi_y \\ \Delta \varphi_z \end{Bmatrix} = \begin{Bmatrix} \Delta u_x^{wh} \\ \Delta u_y^{wh} \\ \Delta u_z^{wh} \\ \Delta \varphi_x^{wh} \\ \Delta \varphi_y^{wh} \\ \Delta \varphi_z^{wh} \end{Bmatrix} - \begin{Bmatrix} \Delta u_x^r \\ \Delta u_y^r \\ \Delta u_z^r \\ \Delta \varphi_x^r \\ \Delta \varphi_y^r \\ \Delta \varphi_z^r \end{Bmatrix}, \quad \text{or} \quad \mathbf{\Delta u} = \mathbf{\Delta u}^{wh} - \mathbf{\Delta u}^r, \tag{2}$$

and correspond to the $\vec{\mathbf{e}}^{C_N}$-system in Figure 2.

The amplitudes of the fluctuating geometry parameters are changed by the amplitudes of the disturbance Δz_ω, Δz_φ and Δz_κ and the amplitudes of the fluctuating relative displacements as follows:

$$\begin{Bmatrix} \Delta d \\ \Delta A \\ \Delta B \\ \Delta \alpha \\ \Delta \xi^c \end{Bmatrix} = \mathbf{G}_{dist} \begin{Bmatrix} \Delta z_w \\ \Delta z_\varphi \\ \Delta z_\kappa \end{Bmatrix} + \mathbf{G}_{disp} \begin{Bmatrix} \Delta u_x \\ \Delta u_y \\ \Delta u_z \\ \Delta \varphi_x \\ \Delta \varphi_y \\ \Delta \varphi_z \end{Bmatrix}, \quad \text{or} \quad \mathbf{\Delta g} = \mathbf{G}_{dist}\mathbf{\Delta z} + \mathbf{G}_{disp}\mathbf{\Delta u}. \tag{3}$$

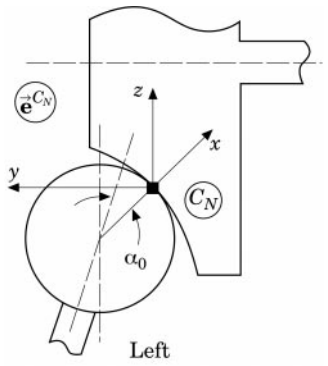

Figure 2. Co-ordinate system for the relative displacements.

A and B are the mean curvatures in the longitudinal and lateral directions respectively. Thus,

$$A = \tfrac{1}{2}(1/[r_0 + \Delta r] + (1/[R_0 + \Delta(1/R)])) \quad \text{and} \quad B = \tfrac{1}{2}(1/R_0^{wh} + 1/[R_0^r + \Delta R^r]),$$

where the lateral wheel radius is assumed to be constant. Then, the linearized fluctuating parts can be derived from the geometry parameters by

$$\Delta A = \tfrac{1}{2}\Delta(1/R) - (1/(2r_0^2))\Delta r \quad \text{and} \quad \Delta B = (1/R_0^{r^2})\Delta R^r.$$

3.2. KINEMATICS

The creepages between wheel and rail are determined from the difference between the components of the wheel and rail velocities at the point of contact with respect to the contact co-ordinate system $\vec{\mathbf{e}}^C$ in Figure 1. One obtains for the amplitudes of the fluctuating creepages

$$\begin{Bmatrix} \Delta\nu_\xi \\ \Delta\nu_\eta \\ \Delta\nu_\zeta \end{Bmatrix} = \mathbf{C}_{disp} \begin{Bmatrix} \Delta u_x \\ \Delta u_y \\ \Delta u_z \\ \Delta\varphi_x \\ \Delta\varphi_y \\ \Delta\varphi_z \end{Bmatrix} + \mathbf{C}_{dist} \begin{Bmatrix} \Delta z_w \\ \Delta z_\varphi \\ \Delta z_\kappa \end{Bmatrix}, \quad \text{or} \quad \mathbf{\Delta\nu} = \mathbf{C}_{disp}\mathbf{\Delta u} + \mathbf{C}_{dist}\mathbf{\Delta z}. \tag{4}$$

3.3. CONTACT MECHANICS

When wheel and rail are in contact, there is an elastic deformation of both bodies due to the static load of the railway vehicle. Thus, a contact patch of the size of a coin exists. The contact forces are transmitted in this contact area. For the amplitude of the fluctuating normal force one may write

$$\Delta N_\zeta = \partial N_\zeta/\partial d(\Delta d) + \partial N_\zeta/\partial A(\Delta A) + \partial N_\zeta/\partial B(\Delta B). \tag{5}$$

Small wavelengths may reduce the effectiveness of the profile irregularity. This can be called the *amplitude filter* effect, for which it is supposed that all three amplitudes of equation (1) are affected; thus

$$\begin{Bmatrix} \Delta z_w \\ \Delta z_\varphi \\ \Delta z_\kappa \end{Bmatrix} = F_{ampli}\left(\frac{1}{L}\right) \begin{Bmatrix} \Delta z_w^{geo} \\ \Delta z_\varphi^{geo} \\ \Delta z_\kappa^{geo} \end{Bmatrix}, \quad \text{or} \quad \mathbf{\Delta z} = F_{ampli}\left(\frac{1}{L}\right)\mathbf{\Delta z}^{geo},$$

where $\mathbf{\Delta z}$ represents the effective profile amplitudes and $\mathbf{\Delta z}^{geo}$ represents the real, geometrically given, profile amplitudes.

The fluctuating linearized contact mechanics, which takes amplitude filter effects as well as transient creepage [5] into account, is described by

$$\begin{Bmatrix} \Delta T_\xi \\ \Delta T_\eta \\ \Delta N_\zeta \\ \Delta M_\zeta \end{Bmatrix} = \mathbf{A}_{con} \begin{Bmatrix} \Delta\nu_\xi \\ \Delta\nu_\eta \\ \Delta\nu_\zeta \\ \Delta d \\ \Delta A \\ \Delta B \\ \Delta\alpha \\ \Delta\xi^c \end{Bmatrix}, \quad \text{or} \quad \mathbf{\Delta f}^c = \mathbf{A}_{con}\mathbf{\Delta k}, \quad \text{with} \quad \mathbf{\Delta k} = \begin{Bmatrix} \mathbf{\Delta\nu} \\ \mathbf{\Delta g} \end{Bmatrix}.$$

3.4. TRANSFORMATION OF THE CONTACT FORCES

From the contact mechanics follow fluctuating contact forces, which refer to the contact coordinate system $\vec{\mathbf{e}}^C$ in Figure 1. These forces and moments act on the rail and wheel and cause fluctuations in relative displacements between wheel and rail. The dynamic motion of wheel and rail is described in co-ordinate systems $\vec{\mathbf{e}}^{WH}$ and $\vec{\mathbf{e}}^R$, which are in general different from the contact system $\vec{\mathbf{e}}^C$ (cf. Figure 3). To calculate the rail and wheel displacements due to the contact forces, one thus has to transform the contact forces into the wheel and rail system by

$$\begin{Bmatrix} \Delta T_x^{WH} \\ \Delta T_y^{WH} \\ \Delta N_z^{WH} \\ \Delta M_x^{WH} \\ \Delta M_y^{WH} \\ \Delta M_z^{WH} \end{Bmatrix} = \mathbf{G}_{\Delta f}^{WH} \begin{Bmatrix} \Delta T_\xi \\ \Delta T_\eta \\ \Delta N_\zeta \\ \Delta M_\zeta \end{Bmatrix} + \mathbf{L}_{red}^{WH} \begin{Bmatrix} \Delta\alpha \\ \Delta\xi^c \end{Bmatrix}, \tag{6}$$

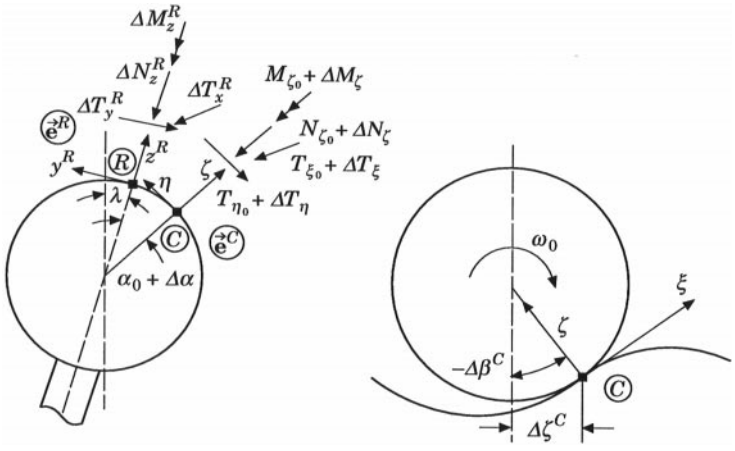

Figure 3. Forces on the rail.

or

$$\mathbf{\Delta f}^{WH} = \mathbf{G}_{\Delta f}^{WH}\mathbf{\Delta f}^{c} + \mathbf{L}^{WH}\mathbf{\Delta k}, \tag{7}$$

and

$$\begin{Bmatrix} \Delta T_x^R \\ \Delta T_y^R \\ \Delta N_z^R \\ \Delta M_x^R \\ \Delta M_y^R \\ \Delta M_z^R \end{Bmatrix} = \mathbf{G}_{\Delta f}^{R} \begin{Bmatrix} \Delta T_\xi \\ \Delta T_\eta \\ \Delta N_\zeta \\ \Delta M_\zeta \end{Bmatrix} + \mathbf{L}_{red}^{R} \begin{Bmatrix} \Delta\alpha \\ \Delta\xi^c \end{Bmatrix}, \tag{8}$$

or

$$\mathbf{\Delta f}^{R} = \mathbf{G}_{\Delta f}^{R}\mathbf{\Delta f}^{c} + \mathbf{L}^{R}\mathbf{\Delta k}. \tag{9}$$

In $\mathbf{L}^{WH}$ and $\mathbf{L}^{R}$ the constant forces T_{ξ_0}, T_{η_0}, N_{ζ_0} and M_{ζ_0} from the reference state are considered.

3.5. WHEEL AND TRACK DYNAMICS

The track model is a frequency domain model using transfer matrices [9]. The rail is described by finite element matrices so that the complex rail profile can be considered. The whole rail is assumed to be infinite and discretely supported by the sleepers. Between the rail and the sleepers there are pads. Under the sleepers is the ballast. Both the pads and the ballast are modelled by linear springs and dampers. The track is excited by a harmonically oscillating load. The position of the load within the sleeper bay can be varied.

The wheel is a finite element model which consists of rotational symmetric shells [10]. The axle is a Timoshenko beam including longitudinal and twisting deformations. Gyroscopic effects can be taken into account but are not considered here.

There are three forces and three moments acting on wheel and rail which may cause three displacements and three rotations of the contact point of each body. This is

$$\begin{Bmatrix} \Delta u_x^{WH} \\ \Delta u_y^{WH} \\ \Delta u_z^{WH} \\ \Delta\varphi_x^{WH} \\ \Delta\varphi_y^{WH} \\ \Delta\varphi_z^{WH} \end{Bmatrix} = \mathbf{D}^{WH} \begin{Bmatrix} \Delta T_x^{WH} \\ \Delta T_y^{WH} \\ \Delta T_z^{WH} \\ \Delta M_x^{WH} \\ \Delta M_y^{WH} \\ \Delta M_z^{WH} \end{Bmatrix} \quad \text{and} \quad \begin{Bmatrix} \Delta u_x^{R} \\ \Delta u_y^{R} \\ \Delta u_z^{R} \\ \Delta\varphi_x^{R} \\ \Delta\varphi_y^{R} \\ \Delta\varphi_z^{R} \end{Bmatrix} = \mathbf{D}^{R} \begin{Bmatrix} \Delta T_x^{R} \\ \Delta T_y^{R} \\ \Delta N_z^{R} \\ \Delta M_x^{R} \\ \Delta M_y^{R} \\ \Delta M_z^{R} \end{Bmatrix},$$

or

$$\Delta\mathbf{u}^{WH} = \mathbf{D}^{WH}\Delta\mathbf{f}^{WH} \quad \text{and} \quad \Delta\mathbf{u}^{R} = \mathbf{D}^{R}\Delta\mathbf{f}^{R}.$$

3.6. TRANSFORMATION OF THE DISPLACEMENTS

Wheel displacements $\Delta\mathbf{u}^{WH}$ and rail displacements $\Delta\mathbf{u}^{R}$, which are caused by the dynamic motion of wheel and rail, correspond to wheel and rail co-ordinate systems $\vec{\mathbf{e}}^{WH}$ and $\vec{\mathbf{e}}^{R}$. To insert these displacements into equations (3) and (4) under consideration of equation (2) they must be transformed into the $\vec{\mathbf{e}}^{C_N}$ system first with

$$\Delta\mathbf{u}^{wh} = \mathbf{G}^{WH}_{\Delta u}\Delta\mathbf{u}^{WH} \quad \text{and} \quad \Delta\mathbf{u}^{c} = \mathbf{G}^{R}_{\Delta u}\Delta\mathbf{u}^{R}.$$

3.7. FEEDBACK LOOP AND STABILITY CRITERION

Figure 4 shows the above given relationships as a feedback loop. Note that

$$\mathbf{C}_{\Delta z} = \begin{bmatrix}\mathbf{C}_{dist}\\ \mathbf{G}_{dist}\end{bmatrix} \quad \text{and} \quad \mathbf{C}_{\Delta u} = \begin{bmatrix}\mathbf{C}_{disp}\\ \mathbf{G}_{disp}\end{bmatrix}.$$

The closed loop of Figure 4 might become unstable. Then, infinitely small input ripples would cause unbounded forces and displacements. This would presumably increase rail corrugation and linearity could no longer be assumed. To avoid this, one must ensure that the closed loop is stable under realistic railway operating conditions. The following stability analysis is an extension of the analysis performed in reference [11]. It is covered in more detail in reference [12].

For the investigation of the stability behaviour a Nyquist stability criterion is used for which the derivation can be found in reference [13].

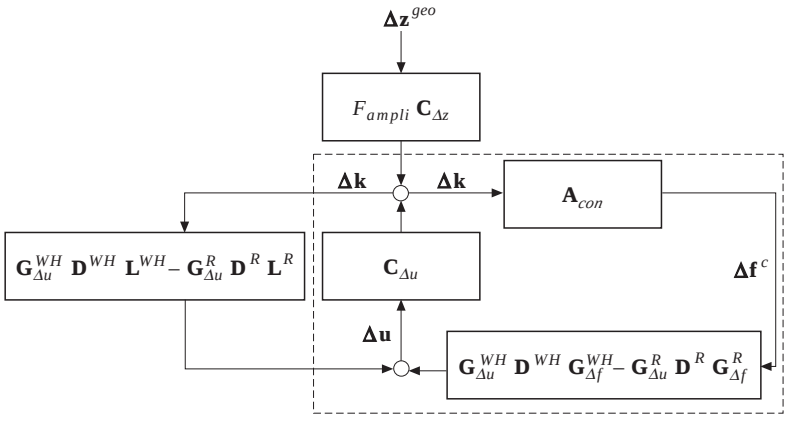

Figure 4. The feedback loop of the transient wheel–track dynamics.

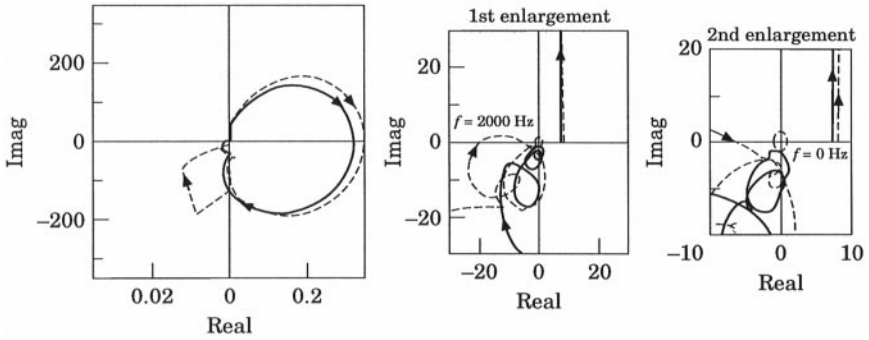

Figure 5. Nyquist plot of the outer loop for a ICE-wheelset on a UIC60 track. —, Sleeper; - - -, midspan.

Nyquist Criterion: *Construct the Nyquist plot of* $\Gamma = \det(\mathbf{I} - \mathbf{K}_1(s)\mathbf{K}_2(s)) - 1$, *indenting to the left around poles on the imaginary axis. Let n denote the total number of poles of* $\mathbf{K}_1$ *and* $\mathbf{K}_2$ *in* $\mathrm{Re}\, s \geqslant 0$. *Then the system is stable iff the Nyquist plot of* Γ *does not pass through the critical point* -1 *and encircles it exactly n times counterclockwise.*

The matrices $\mathbf{K}_1$ and $\mathbf{K}_2$ are $\mathbf{K}_1 = \mathbf{A}_{con}$, and $\mathbf{K}_2 = \mathbf{C}_{\Delta u}\mathbf{D}^{wh-r}$, with $\mathbf{D}^{wh-r} = \mathbf{G}_{\Delta u}^{WH}\mathbf{D}^{WH}\mathbf{G}_{\Delta f}^{WH} - \mathbf{G}_{\Delta u}^{B}\mathbf{D}^{R}\mathbf{G}_{\Delta f}^{R}$, if the feedback due to constant forces of the reference state is neglected. The corresponding closed loop within the dashed rectangle in Figure 4 is called the *outer loop*.

For the *inner loop*, where the outer loop and the feedback due to constant forces are interacting, one obtains $\mathbf{K}_1 = \mathbf{H}_{22}$, and $\mathbf{K}_2 = \mathbf{G}_{\Delta u}^{WH}\mathbf{D}^{WH}\mathbf{L}^{WH} - \mathbf{G}_{\Delta u}^{R}\mathbf{D}^{R}\mathbf{L}^{R}$, with $\mathbf{H}_{22} = [\mathbf{I} - \mathbf{C}_{\Delta u}\mathbf{D}^{wh-r}\mathbf{A}_{con}]^{-1}\mathbf{C}_{\Delta u}$. It can be shown that the whole system remains stable if both the inner and the outer loop are stable [11].

4. STABILITY BEHAVIOUR OF A ICE-WHEELSET ON A UIC60 TRACK

Figure 5 shows the Nyquist plot of the outer loop for a ICE-wheelset on a UIC60 track while the wheel is in midspan and over a sleeper. Note that the Nyquist plot in Figure 5 is calculated at frequencies from 0 to 2000 Hz, while for the application of the Nyquist criterion, as given in section 3.7, a plot at frequencies from $-\infty$ to ∞ is necessary. Since the curves in Figure 5 do not cross the real axis between -1 and 0, however, it can be concluded that the outer loop is stable. It reveals that the inner loop is also stable and thus the whole system remains stable.

5. CALCULATION OF THE WEAR PATTERN

The profile development is calculated by using the frictional energy hypothesis as proposed in reference [14]. It is assumed that the removed mass m per wheel passage n is proportional to the frictional work W_{fric}: $\partial m/\partial n \sim W_{fric}$. It follows for the profile irregularity Δz^{geo}

$$(\partial \Delta z^{geo}/\partial n) = (-k_0/\rho A_{patch})\Delta W_{fric},$$

where k_0 is a proportionality factor, ρ is the density of the removed material and A_{patch} is the area of contact. For the frictional work the same formulation as for the profile irregularity in equation (1) is assumed,

$$\Delta W(x, \eta) = (\Delta W_w + \Delta W_\varphi \eta/b + \Delta W_\kappa(\tfrac{3}{2}(\eta/b)^2 - \tfrac{1}{2}))\, e^{i(2\pi/L)x}.$$

Here the coefficients ΔW_w, ΔW_φ and ΔW_κ can be expressed by Δz_w^{geo}, Δz_p^{geo} and Δz_κ^{geo} again. Then, one has a system of three differential equations:

$$(k_0/\rho)\mathbf{W}_{\Delta z}\Delta z^{geo} + \mathbf{I}\partial/\partial n(\Delta z^{geo}) = 0.$$

$\mathbf{W}_{\Delta z}$ is constant for a given harmonic profile irregularity but varies with the position within a sleeper bay. $\mathbf{I}$ is the unit matrix and Δz^{geo} is the vector of the three profile amplitudes.

At a certain position within a sleeper bay the solution can be written as

$$\Delta z^{geo} = \Delta z_1^{geo}\, e^{\lambda_1 n} + \Delta z_2^{geo}\, e^{\lambda_2 n} + \Delta z_3^{geo}\, e^{\lambda_3 n}. \tag{10}$$

Given disturbances will be amplified if one of the so called *wear rates* $\mathrm{Re}\{\lambda_1\}$, $\mathrm{Re}\{\lambda_2\}$ and $\mathrm{Re}\{\lambda_3\}$ is positive, and suppressed if all are negative.

To determine the profile development due to statistically given profile irregularities, the disturbance must be Fourier analyzed first. The alteration of every harmonic Fourier part after one wheel passage is then governed by equation (10). The sum of all changed Fourier parts after one wheel passage gives the new profile for the next wheel passage. This can be repeated n times which finally gives the amplitudes of the new profile after n wheel passages, and with equation (1) the corresponding wear pattern can be obtained. A more detailed description of this is given in reference [15].

5.1. ANALYSIS OF GEOMETRICAL EFFECTS ON FLUCTUATING WEAR

The formation of short pitch corrugation depends on whether disturbances with a specific wavelength range are amplified or not. To investigate this all three wear rates for a ICE wheelset on a UIC60 track are presented in Figure 6. For these three curves the dynamic motion of wheel and track is omitted. Two things about Figure 6 should be pointed out. First, $\mathrm{Re}\{\lambda_3\}$ will govern the corrugation process since the other two wear rates are negative or comparatively small. Second, the behaviour of $\mathrm{Re}\{\lambda_3\}$ leads to a geometric filter which promotes corrugation growth in a wavelength band between 0·02 and 0·1 m. This geometric filter is independent of vehicle speed. Broadly similar results have been obtained in reference [16]. This is encouraging since the methods of calculation in reference [16] and here are very different.

5.2. WEAR PATTERN FOR A ICE-WHEELSET ROLLING OVER A UIC60 RAIL

In Figures 7 and 8 the wear patterns on the running surface of the rail are presented within a sleeper bay for $v_0 = 50$ m/s and $v_0 = 20$ m/s. In both cases the

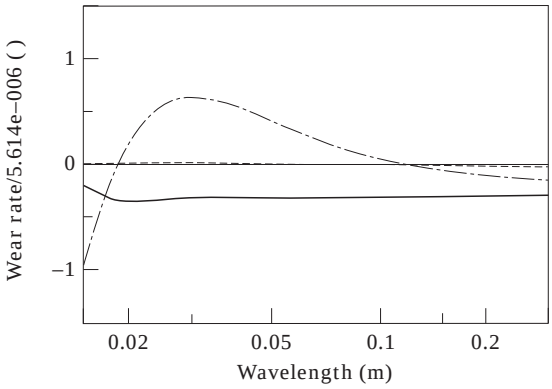

Figure 6. Wear rates (dynamic motion of wheel and track is omitted). —, Re(λ_1); ----, Re(λ_2); –·–·, Re(λ_3).

number of wheel passages is 750 000 and the dynamic motion of the wheelset is omitted. The amplitude spectra of the profile height Δz^{geo} in the middle of both running surfaces, i.e., for $\eta = 0$, are compared in Figure 9. There, it is shown that the maxima of both amplitude spectra are at wavelengths at which Re$\{\lambda_3\}$ from Figure 6 promotes corrugation. For different running speeds different structural dynamics effects are separated out such that the wavelengths of the wear patterns are within a fixed wavelength band. This is explained in more detail by means of Figures 10 and 11.

In Figure 10 the dominant wear rate Re$\{\lambda_3\}$ from Figure 6 is plotted for $v = 20$ m/s, $v = 30$ m/s and $v = 50$ m/s for various frequencies. Below, Figure 11 shows the lateral and vertical receptance of the rail. A strong influence on the wear process of the structural dynamics of the rail can be expected, if characteristic features of the structural dynamics are within a frequency band where the dominant wear rate Re$\{\lambda_3\}$ is maximum.

For $v = 20$ m/s this leads to a strong influence of structural dynamics effects on the wear between 200 and 1000 Hz. Within this frequency range the vertical direct receptance of the rail is minimum at approximately 300 Hz. At this

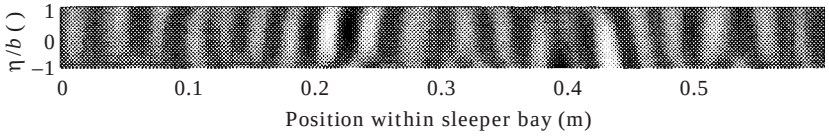

Figure 7. Wear pattern after 750 000 wheel passages for $v = 50$ m/s.

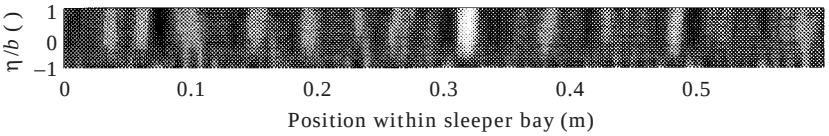

Figure 8. Wear pattern after 750 000 wheel passages for $v = 20$ m/s.

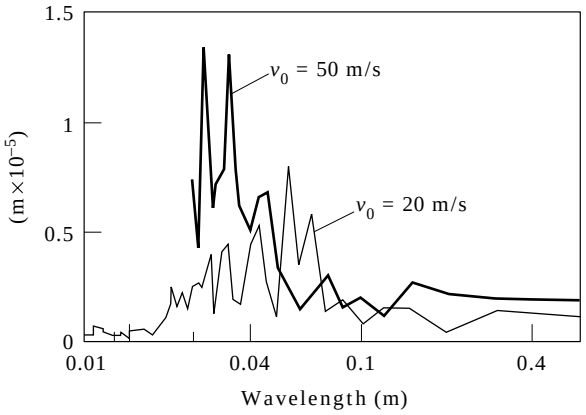

Figure 9. Amplitude curve of $\Delta z^{geo}(\eta = 0)$ for $v_0 = 50$ m/s and $v_0 = 20$ m/s after 750 000 wheel passages.

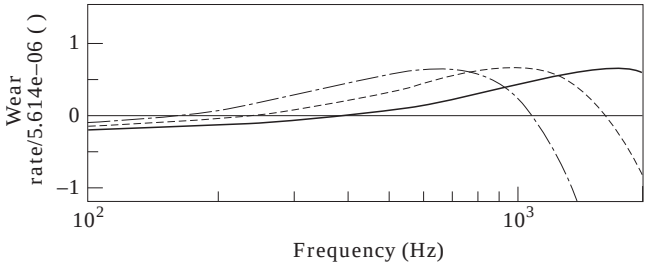

Figure 10. Dominant wear rate for $v = 20$ m/s, $v = 30$ m/s and $v = 50$ m/s (dynamic motion of wheel and track omitted). —, $v_0 = 50$ m/s; - - - -, $v_0 = 30$ m/s; –·–·, $v_0 = 20$ m/s.

frequency the rail is relatively stiff in the vertical direction. This structural dynamics effect promotes corrugation with wavelengths between 6 and 7 cm.

For a vehicle speed of 50 m/s the wear rate in Figure 10 is maximum between 600 and 2000 Hz. At these high frequencies the lateral dynamics dominates the

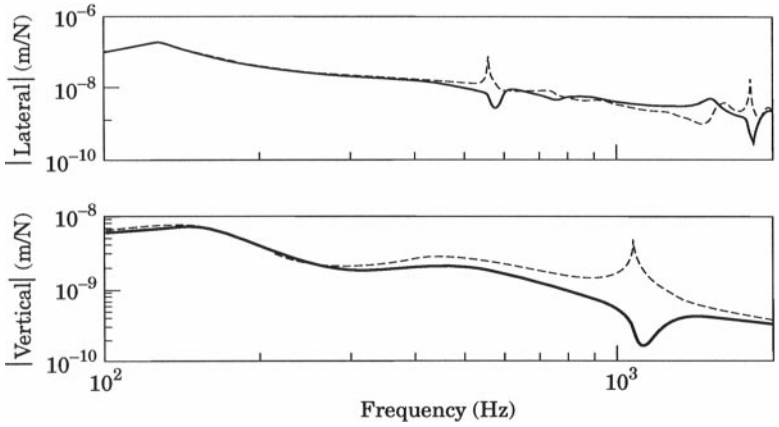

Figure 11. Lateral and vertical direct receptance of a UIC60 rail. —, Sleeper; - - - -, midspan.

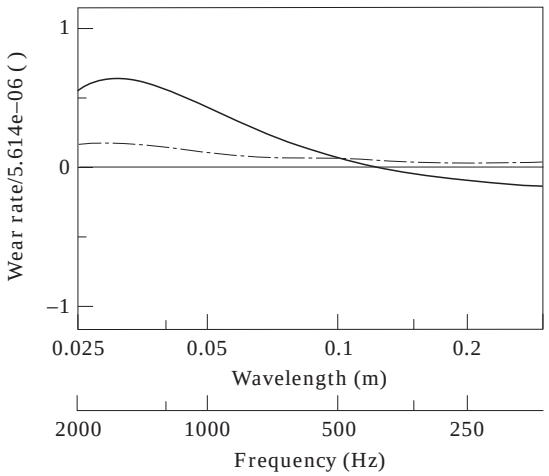

Figure 12. Dominant wear rate for different misalignment angles and wheel radii differences (dynamic motion of wheel and track omitted). –·–·–, $\varphi_z = -0{\cdot}0415°$, $\Delta r = 0$ mm; —, $\varphi_z = -0{\cdot}083°$, $\Delta r = 0{\cdot}67$ mm.

wear process. At 1500 Hz over a sleeper and near 1600 and 1800 Hz in midspan the rail is soft in the lateral direction which promotes corrugation with wavelengths between 2·5 and 3·5 cm.

It might be expected that smaller constant creepages slow down the corrugation process on the rail. Smaller constant creepages can be obtained by reducing the misalignment angle of the wheelset and the difference between the rolling radii of the left and the right wheels.

In Figure 12 the wear rate $\mathrm{Re}\{\lambda_3\}$ of Figure 6 is plotted for different constant creepages. The solid curve has been calculated for a misalignment angle of $-0{\cdot}083°$ and a radii difference of 0·67 mm. For the broken curve the misalignment angle is reduced to $-0{\cdot}0415°$ and the radii difference is zero. For the latter case the resulting profile irregularity is less periodic and in Figure 13 one can see that amplitudes in the wavelength band 2·5–5 cm are clearly reduced.

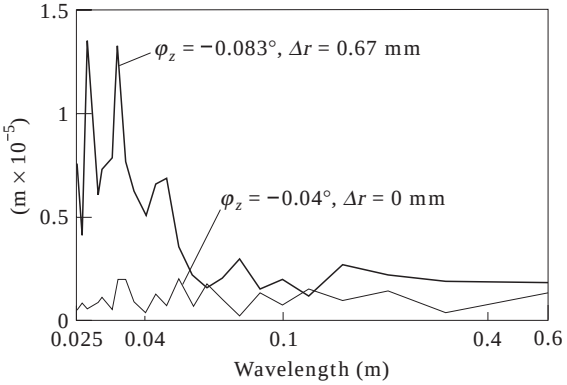

Figure 13. Amplitude curve of Δz^{geo} ($\eta = 0$) for different misalignment angles and wheel radii differences ($v = 50$ m/s, 750 000 wheel passages).

6. CONCLUDING REMARKS

A linear wheel–track model to predict instabilities and the formation of short pitch corrugation has been presented. It comprises the discrete support of the rail, elasticity of the wheelset, all six DOFs of wheel and rail, transient creepage, shift of the contact point and filter effects due to short wavelengths.

It has been shown how a stability analysis can be performed and it has revealed that the investigated ICE-UIC60 combination remains stable. The dynamic motion of the wheelset has been neglected, because its damped eigenmodes made it difficult to determine the number of encirclements of the critical point -1. It remains possible that instability might arise due to wheel resonances. This should be a matter for future research. To avoid the problem mentioned, extending the wheelset model is recommended. It should comprise the primary support, and it should be possible to impose artificial structural damping on the wheelset.

After the stability analysis a wear model has been introduced and it was demonstrated how the profile development due to a high number of wheel passages can be calculated. For the corrugation process, a wavelength-fixing mechanism has been found which could explain the relatively small variation of wavelength of short pitch corrugations. In previous models the low vertical receptance at approximately $f_{fixed} = 1000$ Hz governed the corrugation process. With

$$L = v/f_{fixed} \tag{11}$$

the corrugation wavelength L would vary in direct proportion to the vehicle speed v, whereas the wavelengths observed in practice vary little with train speed.

In this work it has been shown that other structural dynamics effects can also dominate the profile development. A geometrical filter function, which promotes corrugation within a fixed wavelength band, determines which structural dynamics effect is separated out. Thus, the relationship in equation (11) holds, but f is related to different structural dynamics effects such that L is within the wavelength band where the geometrical filter function promotes corrugation.

For the calculation of the wear pattern on the rail only the dynamic motion of the rail has been taken into account while the wheel motion has been neglected. This simplification could be doubtful when the lateral wheel receptance is clearly higher than the lateral receptance of the rail, combined with homogeneous traffic conditions. In this case, it could be possible to have a strong influence on the rail profile development from the wheelset rather than from the rail. This is analyzed in more detail in reference [15].

While here the damage mechanism takes account only of wear caused by friction, at least three additional mechanisms are conceivable. In reference [1] the consideration of plastic deformations generally reduced the wavelength of short pitch corrugation and the corrugation growth seemed to be suppressed. Since the surface on the ridges of profile irregularities is harder than in the troughs [17], the fluctuating wear process might be amplified. On the other hand, measurements showed that the rail surface on ridges is smoother than in troughs which could counteract rail corrugation [18].

REFERENCES

1. C. O. FREDERICK 1987 *Proceedings of the Second International Symposium on Contact Mechanics and Wear of Rail/Wheel Systems held at Kingston/RI, July* 1986; Waterloo/Ontario: University of Waterloo Press, 181–211. A rail corrugation theory.
2. K. HEMPELMANN 1994 *VDI Fortschritt-Berichte* **231** Reihe 12; Düsseldorf: VDI Verlag. Short pitch corrugation on railway rails—a linear model for prediction.
3. S. GRASSIE and J. KALOUSEK 1993 *Proceedings of the Institution of Mechanical Engineers* **207**, *part* F, 57–68. Rail corrugation: characteristics, causes and treatments.
4. A. VALDIVIA 1988 *VDI Fortschritt-Berichte* **93** *Reihe* 12; Düsseldorf: VDI Verlag. Die Wechselwirkung zwischen hochfrequenter Rad-Schiene-Dynamik und ungleichförmigem Schienenverschleiß- ein lineares Modell.
5. A. GROSS-THEBING 1993 *VDI Fortschritt-Berichte* **199** *Reihe* 12; Düsseldorf: VDI Verlag. Lineares Kontaktmodell für ein auf einer wellenförmigen Schienenoberfläche rollendes Rad unter Berücksichtigung einer schwankenden Kontaktfläche.
6. H. ILIAS 1996 *VDI Fortschritt-Berichte* **297** *Reihe* 12; Düsseldorf: VDI Verlag. Nichtlineare Wechselwirkungen von Radsatz und Gleis beim Überrollen von Profilstörungen.
7. J. C. SINCLAIR 1985 *BR Research Report*, *Structures Group*. **RR-STR-95-87**. Rail corrugation development in service.
8. BRITE/EURAM III 96-3017. Silent Track. Development of new technologies for low noise railways infrastructure.
9. B. RIPKE and K. KNOTHE 1991 *VDI Fortschritt-Berichte* **155** *Reihe* 11; Düsseldorf: VDI Verlag. Die unendlich lange Schiene auf diskreten Schwellen bei harmonischer Einzellasterregung.
10. K. KOSE 1997 *Dissertation, TU Berlin*. Berechnung von Eigenschwingungen von Eisenbahnradsätzen mittels Schalenelementen unter Einbeziehung gyroskopischer Effekte.
11. A. BHASKAR, K. JOHNSON and J. WOODHOUSE 1997 *Proceedings of the Institution of Mechanical Engineers* **211** *part* F 11–40. Wheel–rail dynamics with closely conformal contact, part 1: dynamic modelling and stability analysis, part 2: forced response, results and conclusions.
12. S. MÜLLER and K. KNOTHE 1997 *Archive of Applied Mechanics* **67**, 353–363. Stability of wheelset–track dynamics for high frequencies.
13. M. GREEN and D. J. N. LIMEBEER 1995 *Linear Robust Control*. Englewood Cliffs, NJ: Prentice Hall.
14. H. KRAUSE and G. POLL 1986 *Wear* **113**, 103–122. Wear of wheel–rail surfaces.
15. S. MÜLLER 1998 *VDI Fortschritt-Berichte* **369** *Reihe* 12; Düsseldorf: VDI Verlag. Linearized wheel–rail dynamics—stability and corrugation.
16. J. BIRKEDAL NIELSEN Same proceedings. Evolution of rail corrugation predicted with a non-linear wear model.
17. G. BAUMANN 1997 *Dissertation*, *TU Berlin*. Untersuchungen zu Gefügestrukturen und Eigenschaften der "Weissen Schichten" auf verriffelten Schienenlaufflächen.
18. K. KNOTHE and A. THEILER 1997 *Proceedings of the 2nd Mini Conference on Contact Mechanics and Wear of Rail/Wheel Systems*, *Budapest*, *August* 1996 34–43. Normal and tangential contact problem with rough surfaces.